



Output Optical Power Enhancement of Push-Pull Modulated DFB Laser With Asymmetric Structure

Jiewen Chi , Xun Li , Senior Member, IEEE, Chuanning Niu , and Jia Zhao 

Abstract—Conventional push-pull modulated (PPM) distributed feedback (DFB) lasers exploit structures with symmetry, which wastes a significant amount of the optical power output from the rear facet. To improve the power efficiency, PPM DFB lasers with asymmetrically coated facets can be considered. However, the resulted imbalanced push-pull modulation causes a dip in device small-signal intensity modulation response near the carrier-photon resonance (CPR) frequency, which distorts the waveform and even cuts off the bandwidth. This work proposes an asymmetric section length design in conjunction with the asymmetric facet coating to offset the aforementioned effect on device intensity modulation response. With a delayed push-pull modulation (DPPM) scheme further incorporated, our simulation result shows that the PPM DFB laser with optimized asymmetric structure can enhance the power efficiency and maintain a smooth modulation bandwidth up to around 50 GHz.

Index Terms—Asymmetric structure, DFB, intensity modulation response, PPM, slope efficiency.

I. INTRODUCTION

LOW-COST transmitters utilizing directly modulated semiconductor lasers (DMLs) are highly demanded for the high-capacity fiber-optic communication systems [1], [2], [3], [4]. Among the various options, traditional single-sectional distributed feedback (DFB) lasers are preferred due to their simple structure, mature manufacturing technique, and low cost. However, the -3 dB bandwidth associated with the low carrier-photon resonance (CPR) frequency limits their high-speed modulation performance [5], [6]. To solve this problem, many works have been done to optimize the quantum well structure (by, e.g., introducing tensile strain and/or doping the barrier) and reduce the cavity length, since the CPR frequency is proportional to the differential gain and inversely proportional to the cavity length in a square root manner [7], [8], [9], [10]. A transmission rate up to 40 Gbps has been achieved by using such laser source [11], [12], [13]. However, further reduction of the cavity length is restricted by cleaving and thermal dissipating difficulties.

Manuscript received 27 August 2023; accepted 2 September 2023. Date of publication 6 September 2023; date of current version 15 September 2023. (Corresponding author: Xun Li.)

Jiewen Chi, Chuanning Niu, and Jia Zhao are with the School of Information Science and Engineering, Shandong University, Qingdao 266237, China (e-mail: chijiewen@mail.sdu.edu.cn; niuchuanning@sdu.edu.cn; zhaojia@sdu.edu.cn).

Xun Li is with the Department of Electrical and Computer Engineering, McMaster University, Hamilton, ON L8S 4K1, Canada, and also with the School of Information Science and Engineering, Shandong University, Qingdao 266237, China (e-mail: lixun@mcmaster.ca).

Digital Object Identifier 10.1109/JPHOT.2023.3312388

The recent focus of high-speed DMLs has turned to multi-sectional structures that utilize the photon-photon resonance (PPR) effect [14], [15]. The interaction between the lasing and a nearby second mode can happen at a much higher frequency, thereby having the potential to drastically extend the small-signal intensity modulation response [16], [17], [18], [19]. However, the intensity modulation response rapidly decays at the CPR tail, leading to a significant indentation between the PPR and CPR frequencies, which cuts off the bandwidth below PPR. A modulation bandwidth of only 34 GHz was achieved due to the limit set by this cut-off [20]. Various designs that combining the PPR with the detuned-loading effect [21], [22], [23], [24], [25], such as the dual- κ distributed Bragg reflector (DBR) laser with an integrated short semiconductor optical amplifier (SOA), the DFB laser with an integrated passive waveguide, and the distributed reflector (DR) laser with an integrated dual-sectional DBR, can compensate the indentation and further extend the modulation bandwidth to 65 GHz [26].

Nevertheless, all these multiple-sectional DMLs appear to require monolithic integration techniques such as butt-joint regrowth or selective area growth, which makes them less appealing on cost-effectiveness and reliability compared to externally modulated lasers (EMLs) [27], [28], [29], [30], [31], [32], [33], [34].

Yet another alternative approach to generate the PPR effect is the dual-sectional push-pull modulated (PPM) DFB laser. It turns out to be more cost-effective as it does not need any monolithic integration for the device structure in the two sections is identical [35], [36], [37], [38], [39], [40]. We previously studied the PPM DFB laser with a first order grating symmetric cavity structure [41]. The indentation of the intensity modulation response in the frequency band between the CPR and PPR is compensated by introducing a delay between the differential signals applied to the PPM DFB laser. In this work, a second order grating asymmetric cavity structure is investigated. The purpose is to enhance the single-mode yield and the side-mode-suppression-ratio (SMSR), to diminish the aforementioned indentation, and to enhance the output optical power, for the second order grating breaks the degeneracy of the two lasing modes on the Bragg stopband edge [42], its associated radiation expands the PPR peak, and the asymmetric coating applied to the rear and front facets helps to enhance the optical power output. The asymmetric coating design targets to boost the output optical power, however, generates a new issue, i.e., a dip appears in a frequency band slightly lower than CPR peak. With a different root-cause from the indentation studied

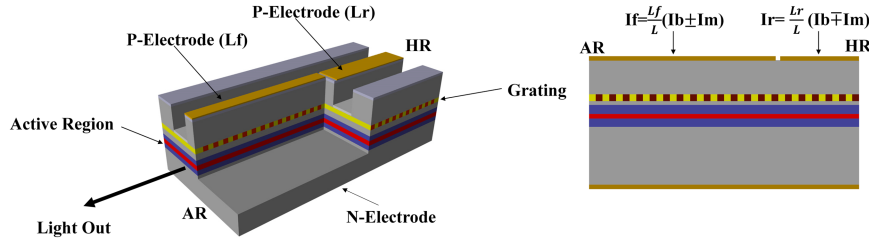


Fig. 1. Schematic of the second order grating asymmetric PPM DFB laser.

in [41], this dip arises from the imbalance between the CPR responses of the rear and front sections due to the asymmetric coating. In an attempt to offset the dip, we further exploited an asymmetric section length design. While we show that the dip can be flattened by an asymmetric coating combined with an optimized asymmetric section length selection, we also find that the delayed push-pull modulation (DPPM) scheme helps to mitigate the dip. Through numerical simulation, we show that a 28% enhancement on the slope efficiency of the power-current (P-I) curve (as compared to the conventional symmetrical PPM DFB laser with a second order grating) is achievable for the second order grating asymmetric PPM DFB laser with a smooth modulation bandwidth up to around 50 GHz.

The rest of the article is organized as follows. In Part II, the effects of asymmetric coating and section length on the device small-signal intensity modulation response are investigated and analyzed; the structure is optimized in Part III; the simulated device performance with an optimized structure is shown in Part IV; this work is finally summarized in Part V.

II. DEPENDENCE OF INTENSITY MODULATION RESPONSE ON ASYMMETRIC STRUCTURE

Fig. 1 shows the schematic of the second order grating asymmetric PPM DFB laser, which shares the similar structure to the conventional single-sectioned DFB laser, with the exception that the top electrode is divided into two electrically insulated segments. The injection currents of the front and rear sections are $I_f = \frac{L_f}{L}(I_b \pm I_m)$ and $I_r = \frac{L_r}{L}(I_b \mp I_m)$, where L_f and L_r are the front and rear section lengths, L the cavity length, and I_b and I_m the DC bias and modulation currents.

A. Simulation Model and Parameters

To investigate the effect of asymmetric coating on the PPM DFB laser characteristics, we exploit an in-house simulation tool based on the well-established one-dimensional traveling wave model (1D TWM) [43], [44]. The description of the 1D TWM can be found in Appendix, and the validity of the simulation tool has been shown in [45], [46].

The intensity modulation response dependence on the DFB laser cavity parameters, such as cavity length and grating coupling coefficient, has been studied in the prior work [41]. In this article, all other laser parameters will remain fixed, except for the facet reflectivities and section lengths. These parameters along with their values used in the simulation are listed in Table I. (Due to the redesign of the device's epitaxial structure, the simulation

TABLE I
PARAMETERS IN LASER SIMULATION

| Symbol | Physical Meaning (Unit) | Values |
|----------------|---|--------|
| Λ | Bragg grating period (nm) | 405 |
| L | Cavity length (μm) | 650 |
| w | Active region width (μm) | 1.6 |
| d | Active region thickness (nm) | 55 |
| R_f | Amplitude reflectivity of front facet | |
| R_r | Amplitude reflectivity of rear facet | |
| h_1 | Surface radiation loss coefficient (cm^{-1}) | 4 |
| κ | Coupling coefficient (cm^{-1}) | 60 |
| Γ | Optical confinement factor | 0.1 |
| n_{eff}^0 | Effective index without injection | 3.222 |
| n_g | Group index | 3.6 |
| α | Optical modal loss (cm^{-1}) | 10 |
| α_{LEF} | Linewidth enhancement factor | 3 |
| a | Differential gain (cm^{-1}) | 1600 |
| N_0 | Transparent carrier density (10^{18}cm^{-3}) | 0.66 |
| ϵ | Nonlinear gain suppression coefficient (10^{-17}cm^3) | 3 |
| τ_c | Carrier lifetime (ns) | 0.5 |

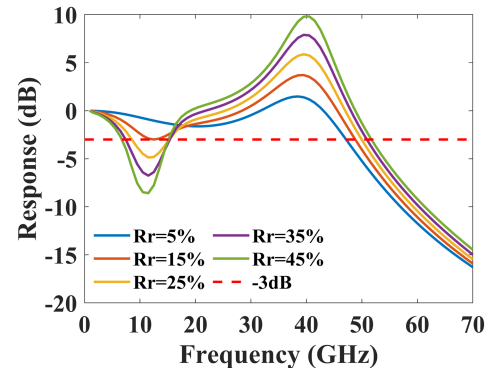


Fig. 2. Effect of rear facet reflectivity on the intensity modulation response obtained from front facet with $R_f = 5\%$, $L_f = L_r$, and $I_b = 53$ mA.

parameter values used in this study differ from those in the prior work.)

B. Dependence of Intensity Modulation Response on Asymmetric Coating

In this section, we reveal the result of the simulated device small-signal intensity modulation response for varying rear facet reflectivities, with a fixed front facet reflectivity (under AR coating) and identical section length.

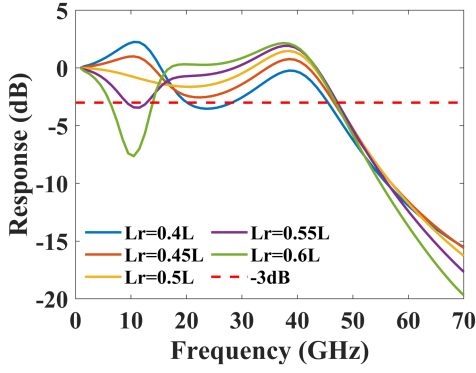


Fig. 3. Effect of section lengths on the intensity modulation response obtained from front facet with $R_f = R_r = 5\%$, $L_f = L - L_r$, and $I_b = 53$ mA.

Fig. 2 shows the dependence of the intensity modulation response for different rear facet reflectivities under a fixed front facet reflectivity at 5% and a DC bias current of 53 mA. If the rear facet reflectivity also equals to 5% (symmetric coating), the response is reasonably smooth within the modulation bandwidth. As the rear facet reflectivity departs from 5%, the coating symmetry is broken, and a dip appears in the intensity modulation response around 10 GHz. As the rear facet reflectivity increases, the dip is deeper and slightly moves towards the lower frequency side. The unflatness of the response jeopardizes the eye-diagram. With further rising of the rear facet reflectivity, the dip can even cut off the modulation bandwidth and limit it to the neighborhood of 10 GHz.

The symmetry broken of the facet reflectivity results in an asymmetric optical field distribution between the front and rear sections. Considering that the modulation current is a signal in differential mode, the CPR response of the front section is out of phase with that of the rear section. This asymmetric optical field distribution within the cavity results in an imbalance between the CPR responses of the front and rear sections, which causes the dip as the intensity modulation response could be cancelled to each other due to the phase difference between the responses from the front and rear sections. The more serious the asymmetry of the optical field distribution is, the greater imbalance between the CPR responses will be, which will generally cause a deeper dip in the intensity modulation response obtained from the front facet.

C. Dependence of Intensity Modulation Response on Asymmetric Section Length

Based on the above analysis, we consider that using different front and rear section lengths would also disrupt the balance between the CPR responses, as not only the asymmetric facet coating, but also the section length, can effectively change the optical field distribution along the DFB laser cavity. Again, we reveal the result of the simulated device small-signal intensity modulation response for varying section lengths, with symmetrical coating on both facets.

Fig. 3 shows the dependence of the intensity modulation response for different rear section lengths under a DC bias of

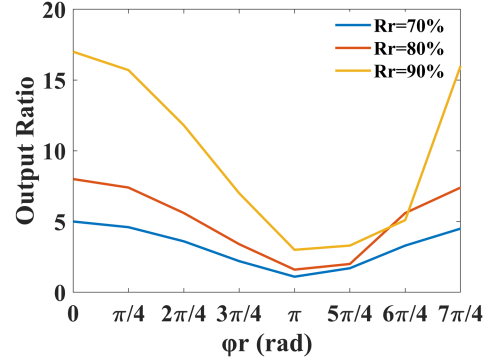


Fig. 4. Effect of rear facet reflectivity and phase on the output power ratio with $R_f = 5\%$.

53 mA, with a fixed total cavity length and a reflectivity of 5% for both facets. If the rear and front section lengths are equal (each takes the half of the total cavity length), the response is reasonably smooth within the modulation bandwidth. As the rear section length departs from half of the total length, the symmetry is broken, and a dip or a bump appears in the intensity modulation response around 10 GHz, depending on the rear section length is longer or shorter. Apparently, it is possible to offset the imbalance between the CPR responses caused by the asymmetric coating by appropriately adjusting section lengths.

It can also be summarized that a dip will appear once the photons have a relatively longer lifetime in the rear than in the front section, and a bump will appear vice versa, for the increased facet reflection and section length tend to retain the photons longer inside the cavity. A combination of higher rear facet reflection and shorter rear section length can therefore possibly raise the output optical power from the front facet and meanwhile keep a flat response inside the modulation bandwidth.

III. OPTIMIZED STRUCTURE

A. Optimum Reflectivity

The relationship between the ratio of the power output from the front facet (which is AR coated with a reflectivity of 5%) to that output from the rear facet and the reflectivity and phase (φ_r) of the rear facet, is illustrated in Fig. 4. It can be observed that the overall trend of the output ratio increases with the rise in the reflectivity of the rear facet. This trend indicates that increasing the reflectivity of the rear facet will improve the power efficiency of the device.

For the purpose of improving the power efficiency, we prefer to have a facet reflection at the rear end as high as possible. However, an excessively high reflective coating will jeopardize the single-mode yield. Eight equidistant values ranging from 0 to 2π are selected as the rear facet phases, and the single-mode yield is defined as the proportion of cases in which the SMSR exceeds 30 dB among these phases. Fig. 5 shows the numerically simulated dependence of the device's single-mode yield on the rear facet reflection under a bias current of 80 mA, when the device's front facet is AR coated with a reflectivity of 5%. It can be found that the single-mode yield drops abruptly from

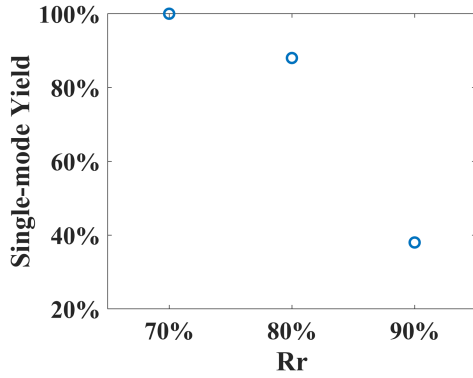


Fig. 5. Effect of rear facet reflectivity on the single-mode yield with $R_f = 5\%$ and $I_b = 80$ mA.

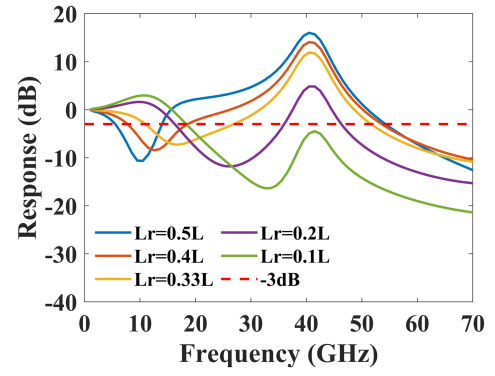


Fig. 7. Effect of section lengths on the intensity modulation response obtained from front facet with $R_f = 5\%$, $R_r = 80\%$, $L_f = L - L_r$, and $I_b = 53$ mA.

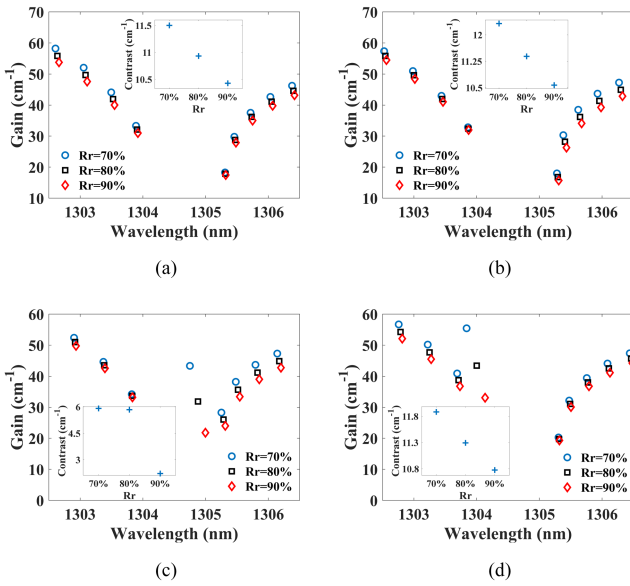


Fig. 6. Effect of rear facet reflectivity on the threshold mode gain distribution with $R_f = 5\%$, (a) $\varphi_r = 1/4\pi$, (b) $\varphi_r = 3/4\pi$, (c) $\varphi_r = 5/4\pi$, (d) $\varphi_r = 7/4\pi$. (The inset shows the contrast between the lowest and the second lowest threshold gains).

88% to 38% when the rear facet reflectivity increases from 80% to 90%. Fig. 6 shows the dependence of the threshold mode gain distribution for different rear facet reflectivities under a fixed front facet reflectivity at 5%. When the intracavity gain exceeds the threshold gain of a certain mode, that mode will start lasing. As the reflectivity of the rear facet increases, the contrast between the lowest and the second lowest threshold gains diminishes, which makes the second mode more prone to lasing, resulting in a deterioration of the device's single-mode stability.

Therefore, we choose the rear facet reflectivity as 80% to achieve a relatively high power efficiency while maintaining a reasonably good single-mode yield. For analytical convenience, the phase of the rear facet is set to 0 in the following work.

B. Optimum Section Length

The simulated intensity modulation responses under different section lengths is shown in Fig. 7, when the front AR and

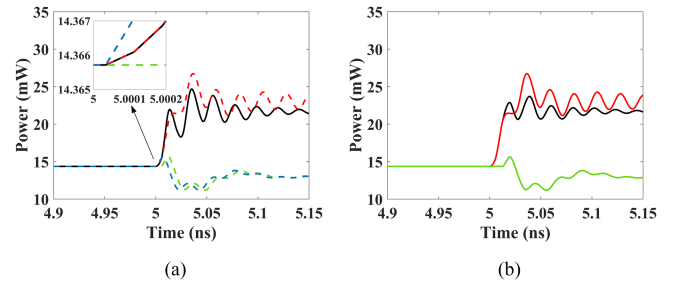


Fig. 8. Time-domain response output from front facet, (a) without time delay, (b) with a 7.5 ps time delay. (The inset shows the magnified response times).

rear HR coated facet reflectivities are set as 5% and 80%, respectively. It can be observed that when the front and rear sections are of equal length, a deep dip appears at around 10 GHz. As the rear section length decreases, the dip is gradually compensated and eventually transforms into a bump. However, the overly decreased rear section length weakens the PPM effect and destroys its PPR, making the intensity modulation response increasingly similar to that of the conventional DML with a retreated modulation bandwidth. To minimize this dip in the intensity modulation response without causing much retreat of the bandwidth, the rear section length is selected as $0.33L$, hence the front section length is $0.67L$.

C. Optimum Delay Time

To further fill up this dip, the DPPM scheme was incorporated. Since the flatness of the time-domain output response is closely related to that of the intensity modulation response, the required delay time can be estimated by smoothing the time-domain output response [47]. The time-domain output response of the PPM DFB laser is approximated as the sum of the front and rear section responses. Fig. 8(a) shows the PPM response without delay time, along with the front and rear section responses. The solid black line represents the PPM response obtained by transforming $I_f = \frac{L_f}{L} I_b$ to $I_f = \frac{L_f}{L} (I_b + I_m)$ at $\tau_{mf} = 5$ ns, and $I_r = \frac{L_r}{L} I_b$ to $I_r = \frac{L_r}{L} (I_b - I_m)$ at $\tau_{mr} = 5$ ns, where τ_{mf} and τ_{mr} are the modulated current injection times of the front and rear sections. The dotted red line represents the

front section response obtained by transforming $I_f = \frac{L_f}{L} I_b$ to $I_f = \frac{L_f}{L} (I_b + I_m)$ at $\tau_{mf} = 5$ ns, while maintaining $I_r = \frac{L_r}{L} I_b$. The dotted green line represents the rear section response obtained by transforming $I_r = \frac{L_r}{L} I_b$ to $I_r = \frac{L_r}{L} (I_b - I_m)$ at $\tau_{mr} = 5$ ns, while maintaining $I_f = \frac{L_f}{L} I_b$. The dotted blue line represents the rear section response obtained by transforming $I_r = \frac{L_r}{L} I_b$ to $I_r = \frac{L_r}{L} (I_b - I_m)$ at $\tau_{mr} = 4.9948$ ns, while maintaining $I_f = \frac{L_f}{L} I_b$. The oscillation frequencies of these responses are approximately equal to the PPR frequency. Since the response of the rear section must propagate through the front section before exiting from the front facet, it is slower than both the PPM and front section responses. This time contrast corresponds to the propagation time of light in the front section. The optimized length of the front section is approximately 435 μm ($L = 650 \mu\text{m}$, $L_f = 0.67L$, and $L_r = 0.33L$), resulting in a propagation time of about 5.2 ps. By advancing the modulated current injection time of the rear section by 5.2 ps, it is evident that the response time of the rear section matches that of both the PPM and front section. At this moment, the response of the rear section is almost in phase with that of the front section. To achieve a smooth PPM response, the phase of the rear section response needs to differ by approximately π from that of the front section response, requiring a delay of about half a PPR cycle for the rear section response. As the PPR frequency is 40 GHz, the required delay time (τ_d) is about 12.5 ps. However, considering that the rear section response already has a 5.2 ps time delay compared to the front section response, the actual required delay time is about 7.5 ps.

In Fig. 8(b), a 7.5 ps delay time was introduced into the modulated current of the rear section. The solid black line represents the PPM response obtained by transforming $I_f = \frac{L_f}{L} I_b$ to $I_f = \frac{L_f}{L} (I_b + I_m)$ at $\tau_{mf} = 5$ ns, and $I_r = \frac{L_r}{L} I_b$ to $I_r = \frac{L_r}{L} (I_b - I_m)$ at $\tau_{mr} = 5.0075$ ns. The solid red line represents the front section response obtained by transforming $I_f = \frac{L_f}{L} I_b$ to $I_f = \frac{L_f}{L} (I_b + I_m)$ at $\tau_{mf} = 5$ ns, while maintaining $I_r = \frac{L_r}{L} I_b$. The solid green line represents the rear section response obtained by transforming $I_r = \frac{L_r}{L} I_b$ to $I_r = \frac{L_r}{L} (I_b - I_m)$ at $\tau_{mr} = 5.0075$ ns, while maintaining $I_f = \frac{L_f}{L} I_b$. Under this condition, the response of the rear section is nearly out of phase with that of the front section. As a result, the oscillation of the PPM response is significantly damped with such a time delay, as evidenced by the comparison of the PPM responses (the solid black line) in Fig. 8(a) and (b). In conclusion, the delay time can be estimated by $\tau_d = 1/(2f_{PPR}) - \tau_f$, where f_{PPR} is the PPR frequency and τ_f the propagation time of light in the front section.

For a more accurate optimum delay time, we performed a numerical simulation. The simulated intensity modulation responses of the asymmetrically coated structure with optimized section length at various delay times are shown in Fig. 9. It is evident that within the delay time range of 6 to 10 ps, the dip can be effectively compensated. The above estimated delay time falls within this range. We selected 6 ps as the optimum delay time since it corresponds to the largest modulation bandwidth.

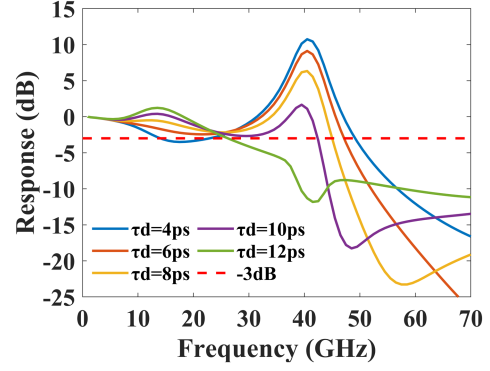


Fig. 9. Effect of delay time on the intensity modulation response obtained from front facet with $R_f = 5\%$, $R_r = 80\%$, $L_f = 0.67L$, $L_r = 0.33L$, and $I_b = 53$ mA.

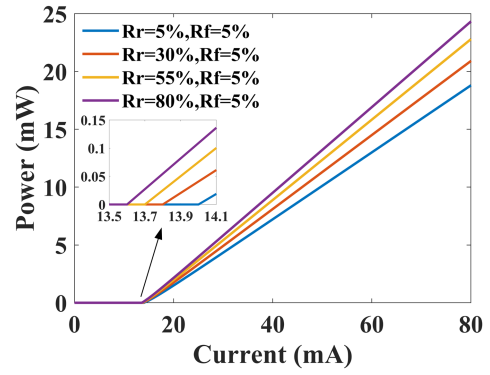


Fig. 10. P-I curves of the symmetrically and asymmetrically coated structures. (The inset shows the magnified threshold currents).

IV. DEVICE PERFORMANCE

Fig. 10 shows the P-I dependence of the optimized asymmetric structure with its rear/front facet HR/AR coated to 80%/5% and with its rear/front section length taken 33%/67% of the total device length. The P-I dependences of the structures with rear/front facet coatings of 5%/5%, 30%/5%, and 55%/5% are also shown in the same figure for comparison. The maximum simulated slope efficiency of the asymmetrically coated structure is 0.36 mW/mA when the rear/front facet is coated to 80%/5%, whereas that of the symmetrically coated structure is 0.28 mW/mA. The asymmetrically coated structure leads to a 28% enhancement on the slope efficiency compared to the symmetrically coated structure. If the reflectivity of the front facet is further reduced, the slope efficiency can be further improved. The lasing wavelength of the optimized asymmetric structure is approximately 1305.3 nm, as shown in Fig. 11.

Fig. 12 shows the simulated intensity modulation response of the symmetric structure (a), the asymmetrically coated structure with identical section length (b), the optimized asymmetric structure (c), the asymmetrically coated structure with identical section length incorporating DPPM (d), and the optimized asymmetric structure incorporating DPPM (e). As demonstrated in Fig. 12(e), the dip is completely compensated by further

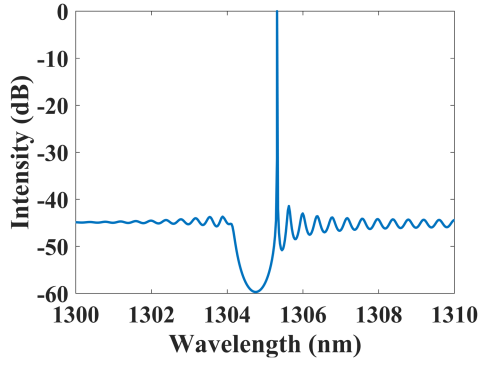


Fig. 11. Lasing spectrum of the optimized asymmetric structure.

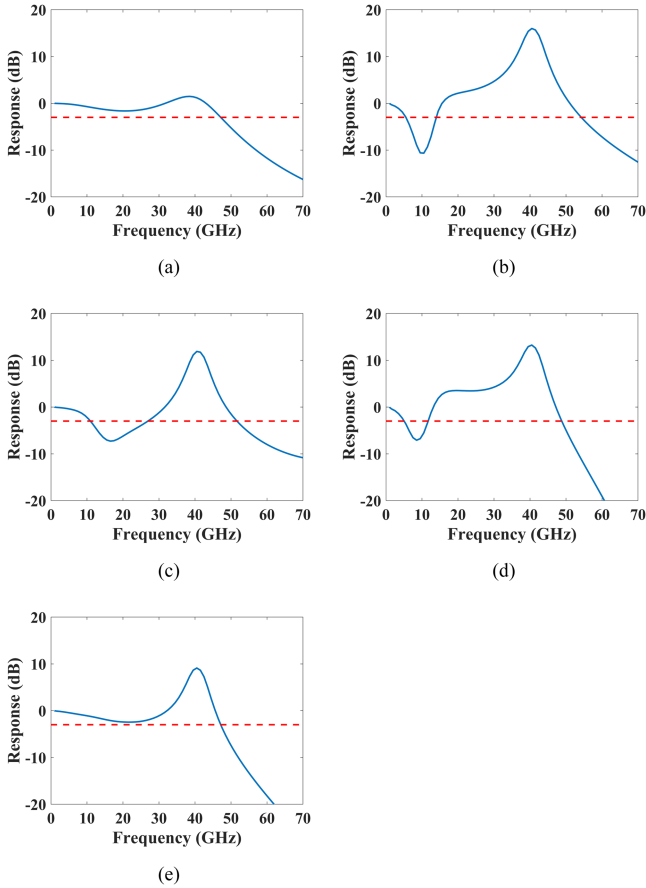


Fig. 12. Intensity modulation response obtained from front facet with $I_b = 53$ mA, (a) $R_f = 5\%$, $R_r = 5\%$, $L_f = 0.5L$, $L_r = 0.5L$, and $\tau_d = 0$ ps, (b) $R_f = 5\%$, $R_r = 80\%$, $L_f = 0.5L$, $L_r = 0.5L$, and $\tau_d = 0$ ps, (c) $R_f = 5\%$, $R_r = 80\%$, $L_f = 0.67L$, $L_r = 0.33L$, and $\tau_d = 0$ ps, (d) $R_f = 5\%$, $R_r = 80\%$, $L_f = 0.5L$, $L_r = 0.5L$, and $\tau_d = 6$ ps, (e) $R_f = 5\%$, $R_r = 80\%$, $L_f = 0.67L$, $L_r = 0.33L$, and $\tau_d = 6$ ps.

introducing a 6 ps modulation delay time to the optimized asymmetric structure, resulting in a smooth intensity modulation response up to approximately 50 GHz.

The large-signal responses of the five aforementioned structures were simulated using 50 Gbps NRZ signals with a peak-to-peak modulation current of $0.5I_b$. Fig. 13 shows the eye-diagram of the symmetric structure (a), the asymmetrically

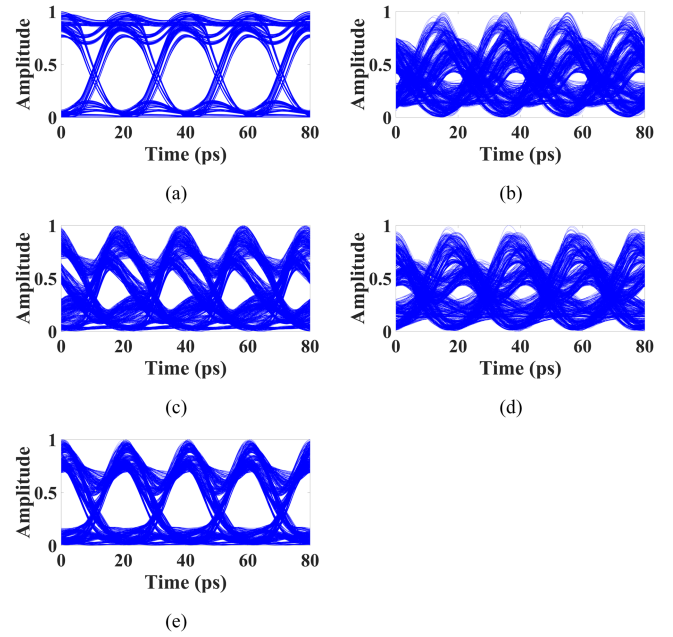


Fig. 13. 50 Gbps NRZ eye-diagram obtained from front facet with $I_b = 53$ mA, (a) $R_f = 5\%$, $R_r = 5\%$, $L_f = 0.5L$, $L_r = 0.5L$, and $\tau_d = 0$ ps, (b) $R_f = 5\%$, $R_r = 80\%$, $L_f = 0.5L$, $L_r = 0.5L$, and $\tau_d = 0$ ps, (c) $R_f = 5\%$, $R_r = 80\%$, $L_f = 0.67L$, $L_r = 0.33L$, and $\tau_d = 0$ ps, (d) $R_f = 5\%$, $R_r = 80\%$, $L_f = 0.5L$, $L_r = 0.5L$, and $\tau_d = 6$ ps, (e) $R_f = 5\%$, $R_r = 80\%$, $L_f = 0.67L$, $L_r = 0.33L$, and $\tau_d = 6$ ps.

coated structure with identical section length (b), the optimized asymmetric structure (c), the asymmetrically coated structure with identical section length incorporating DPPM (d), and the optimized asymmetric structure incorporating DPPM (e). It is clear that the restored quality of the eye-diagram is attributed to the design optimization of the device structure, which leads to a smooth intensity modulation response in the optimized asymmetric structure. Additionally, it is worth mentioning that despite the slightly worse eye-diagram, the average power of the optimized asymmetric structure's eye-diagram is approximately 30% higher than that of the symmetric structure.

V. CONCLUSION

In this work, PPM DFB lasers with asymmetrically coated facets are proposed for improving the power efficiency. To mitigate the effect of the broken symmetry to the smoothness of the intensity modulation response, an asymmetric section length design is further exploited. Through numerical simulations, we show that the optimized asymmetric structure with the DPPM scheme incorporated, can achieve a 28% increase on the slope efficiency of the laser P-I curve compared to the symmetric structure without DPPM, with a smooth modulation bandwidth up to approximately 50 GHz. This design is promising for light sources in applications such as high-speed intra and inter-data center connections, where power efficiency and cost-effectiveness are crucial considerations, for it only requires mature fabrication technology.

APPENDIX

The slowly varying envelopes $F(z, t)$ and $R(z, t)$ of the forward and backward propagating waves are governed by the following equations:

$$\begin{aligned} & \left(\frac{1}{v_g} \frac{\partial}{\partial t} + \frac{\partial}{\partial z} \right) F(z, t) \\ &= \left\{ -j\delta + \frac{1}{2} \left[\frac{\Gamma g(z, t)}{1 + \varepsilon P_s(z, t)} - \alpha \right] - h_1 \right\} \cdot F(z, t) \\ &+ j(\kappa + jh_1) R(z, t) + \tilde{s}^f(z, t), \end{aligned} \quad (\text{A1})$$

$$\begin{aligned} & \left(\frac{1}{v_g} \frac{\partial}{\partial t} - \frac{\partial}{\partial z} \right) R(z, t) \\ &= \left\{ -j\delta + \frac{1}{2} \left[\frac{\Gamma g(z, t)}{1 + \varepsilon P_s(z, t)} - \alpha \right] - h_1 \right\} \cdot R(z, t) \\ &+ j(\kappa + jh_1) F(z, t) + \tilde{s}^r(z, t), \end{aligned} \quad (\text{A2})$$

where $v_g = c/n_g$ is the group velocity, c the speed of the light, n_g the group index, j the imaginary unit, Γ the optical confinement factor, ε the nonlinear gain suppression coefficient, α the optical modal loss, h_1 the surface radiation loss coefficient, κ the coupling coefficient, and $\tilde{s}^f(z, t)$ and $\tilde{s}^r(z, t)$ the spontaneous emission noise fields.

The phase detuning factor from the Bragg wavelength is:

$$\delta = \frac{2\pi n_{eff}^0}{\lambda_0} - \frac{1}{2} \alpha_{LEF} \Gamma g(z, t) - \frac{2\pi}{\Lambda}, \quad (\text{A3})$$

where n_{eff}^0 is the effective index without injection, λ_0 the peak gain wavelength, α_{LEF} the linewidth enhancement factor, and Λ the Bragg grating period.

For the quantum well active region, the analytical expression of the material optical gain is:

$$g(z, t) = a \ln \left[\frac{N(z, t)}{N_0} \right], \quad (\text{A4})$$

where a is the differential gain and N_0 the transparent carrier density.

The photon density distribution in the laser cavity is:

$$P_s(z, t) = \frac{n_{eff}}{2\hbar v_0} \sqrt{\frac{\varepsilon_0}{\mu_0}} \frac{\Gamma}{dw v_g} \cdot \left[|F(z, t)|^2 + |R(z, t)|^2 \right], \quad (\text{A5})$$

where $n_{eff} = n_{eff}^0 - \lambda_0 \alpha_{LEF} \Gamma g(z, t) / 4\pi$ is the effective index, \hbar the Planck's constant, v_0 the optical frequency corresponding to λ_0 , ε_0 the permittivity of a vacuum, μ_0 the permeability of a vacuum, d the thickness of active region, and w the width of active region.

For the carrier density distribution in the laser cavity, the rate equation model is used:

$$\frac{dN(z, t)}{dt} = \frac{I(t)}{eV} - \frac{N(z, t)}{\tau_c} - \frac{v_g P_s(z, t) g(z, t)}{1 + \varepsilon P_s(z, t)}, \quad (\text{A6})$$

where $I(t)$ is the injected current, e the electron charge, V the active region volume, and τ_c the carrier lifetime.

REFERENCES

- [1] Y. Matsui, T. Pham, T. Sudo, G. Carey, and B. Young, "112-Gb/s WDM link using two directly modulated Al-MQW BH DFB lasers at 56 Gb/s," in *Proc. IEEE Opt. Fiber Commun. Conf. Exhib.*, 2015, pp. 1–3.
- [2] R. Motaghianezam et al., "52 Gbps PAM4 receiver sensitivity study for 400GBase-LR8 system using directly modulated laser," *Opt. Exp.*, vol. 24, no. 7, pp. 7374–7380, 2016, doi: [10.1364/OE.24.007374](https://doi.org/10.1364/OE.24.007374).
- [3] C. F. Lam, H. Liu, B. Koley, X. Zhao, V. Kamalov, and V. Gill, "Fiber optic communication technologies: What's needed for datacenter network operations," *IEEE Commun. Mag.*, vol. 48, no. 7, pp. 32–39, Jul. 2010, doi: [10.1109/MCOM.2010.5496876](https://doi.org/10.1109/MCOM.2010.5496876).
- [4] N. Sasada et al., "Wide-temperature-range (25–80°C) 53-gbaud PAM4 (106-Gb/s) operation of 1.3- μm directly modulated DFB lasers for 10-km transmission," *J. Lightw. Technol.*, vol. 37, no. 7, pp. 1686–1689, Apr. 2019, doi: [10.1109/JLT.2019.2894173](https://doi.org/10.1109/JLT.2019.2894173).
- [5] M. N. Akram, C. Silfvenius, O. Kjebon, and R. Schatz, "Design optimization of InGaAsP-InGaAlAs 1.55 μm strain-compensated MQW lasers for direct modulation applications," *Semicond. Sci. Technol.*, vol. 19, no. 5, pp. 615–625, 2004, doi: [10.1088/0268-1242/19/5/010](https://doi.org/10.1088/0268-1242/19/5/010).
- [6] K. Nakahara et al., "High extinction ratio operation at 40-gb/s direct modulation in 1.3- μm InGaAlAs-MQW RWG DFB lasers," in *Proc. IEEE Opt. Fiber Commun. Conf. Nat. Fiber Optic Engineers Conf.*, 2006, pp. 1–3.
- [7] Y. Matsui, H. Murai, S. Arahira, S. Kutsuzawa, and Y. Ogawa, "30-GHz bandwidth 1.55- μm strain-compensated InGaAlAs-InGaAsP MQW laser," *IEEE Photon. Technol. Lett.*, vol. 9, no. 1, pp. 25–27, Jan. 1997, doi: [10.1109/68.554159](https://doi.org/10.1109/68.554159).
- [8] S. R. Selmic et al., "Design and characterization of 1.3- μm AlGaInAs-InP multiple-quantum-well lasers," *IEEE J. Sel. Topics Quantum Electron.*, vol. 7, no. 2, pp. 340–349, Mar./Apr. 2001, doi: [10.1109/2944.954148](https://doi.org/10.1109/2944.954148).
- [9] K. Nakahara et al., "12.5-Gb/s direct modulation up to 115°C in 1.3- μm InGaAlAs-MQW RWG DFB lasers with notch-free grating structure," *J. Lightw. Technol.*, vol. 22, no. 1, pp. 159–165, Jan. 2004, doi: [10.1109/JLT.2003.822157](https://doi.org/10.1109/JLT.2003.822157).
- [10] T. Nakamura et al., "1.3- μm AlGaInAs strain compensated MQW-buried-heterostructure lasers for uncooled 10-gb/s operation," *IEEE J. Sel. Topics Quantum Electron.*, vol. 11, no. 1, pp. 141–147, Jan./Feb. 2005, doi: [10.1109/JSTQE.2004.841691](https://doi.org/10.1109/JSTQE.2004.841691).
- [11] K. Nakahara et al., "40-Gb/s direct modulation with high extinction ratio operation of 1.3- μm InGaAlAs multi-quantum well ridge waveguide distributed feedback lasers," *IEEE Photon. Technol. Lett.*, vol. 19, no. 19, pp. 1436–1438, Oct. 2007, doi: [10.1109/LPT.2007.903530](https://doi.org/10.1109/LPT.2007.903530).
- [12] T. Tadokoro, W. Kobayashi, T. Fujisawa, T. Yamanaka, and F. Kano, "43 Gb/s 1.3 μm DFB laser for 40 km transmission," *J. Lightw. Technol.*, vol. 30, no. 15, pp. 2520–2524, Aug. 2012, doi: [10.1109/JLT.2012.2203095](https://doi.org/10.1109/JLT.2012.2203095).
- [13] B. Huiszoon, R. J. W. Jonker, P. K. van Bennekorn, G.-D. Khoe, and H. de Waardt, "Cost-effective up to 40 Gb/s transmission performance of 1310 nm directly modulated lasers for short- to medium-range distances," *J. Lightw. Technol.*, vol. 23, no. 3, pp. 1116–1125, Mar. 2005, doi: [10.1109/JLT.2004.841435](https://doi.org/10.1109/JLT.2004.841435).
- [14] U. Feiste, "Optimization of modulation bandwidth in DBR lasers with detuned Bragg reflectors," *IEEE J. Quantum Electron.*, vol. 34, no. 12, pp. 2371–2379, Dec. 1998, doi: [10.1109/3.736110](https://doi.org/10.1109/3.736110).
- [15] J. P. Reithmaier et al., "Modulation speed enhancement by coupling to higher order resonances: A road towards 40 GHz bandwidth lasers on InP," in *Proc. Int. Conf. Indium Phosphide Related Mater.*, 2005, pp. 118–123.
- [16] A. A. Tager and K. Petermann, "High-frequency oscillations and self-mode locking in short external-cavity laser diodes," *IEEE J. Quantum Electron.*, vol. 30, no. 7, pp. 1553–1561, Jul. 1994, doi: [10.1109/3.299487](https://doi.org/10.1109/3.299487).
- [17] H. Wenzel, U. Bandelow, H.-J. Wunsche, and J. Rehberg, "Mechanisms of fast self-pulsations in two-section DFB lasers," *IEEE J. Quantum Electron.*, vol. 32, no. 1, pp. 69–78, Jan. 1996, doi: [10.1109/3.481922](https://doi.org/10.1109/3.481922).
- [18] O. Brox et al., "High-frequency pulsations in DFB lasers with amplified feedback," *IEEE J. Quantum Electron.*, vol. 39, no. 11, pp. 1381–1387, Nov. 2003, doi: [10.1109/JQE.2003.818313](https://doi.org/10.1109/JQE.2003.818313).
- [19] S. Bauer et al., "Nonlinear dynamics of semiconductor lasers with active optical feedback," *Phys. Rev. E*, vol. 69, no. 1, 2004, Art. no. 10-016206, doi: [10.1103/PhysRevE.69.016206](https://doi.org/10.1103/PhysRevE.69.016206).
- [20] J. Kreissl, V. Vercesi, U. Troppenz, T. Gaertner, W. Wenisch, and M. Schell, "Up to 40 Gb/s directly modulated laser operating at low driving current: Buried-heterostructure passive feedback laser (BH-PFL)," *IEEE Photon. Technol. Lett.*, vol. 24, no. 5, pp. 362–364, Mar. 2012, doi: [10.1109/LPT.2011.2179530](https://doi.org/10.1109/LPT.2011.2179530).

- [21] K. Vahala and A. Yariv, "Detuned loading in coupled cavity semiconductor lasers - effect on quantum noise and dynamics," *Appl. Phys. Lett.*, vol. 45, no. 5, pp. 501–503, 1984, doi: [10.1063/1.95316](https://doi.org/10.1063/1.95316).
- [22] Y. Matsui et al., "55-GHz bandwidth short-cavity distributed reflector laser and its application to 112-gb/s PAM-4," in *Proc. IEEE Opt. Fiber Commun. Conf. Exhib.*, 2016, pp. 1–3.
- [23] M. Chaciński and R. Schatz, "Impact of losses in the Bragg section on the dynamics of detuned loaded DBR lasers," *IEEE J. Quantum Electron.*, vol. 46, no. 9, pp. 1360–1367, Sep. 2010, doi: [10.1109/JQE.2010.2048013](https://doi.org/10.1109/JQE.2010.2048013).
- [24] O. Kjebon, R. Schatz, S. Lourdudoss, S. Nilsson, B. Stalnacke, and L. Backbom, "30 GHz direct modulation bandwidth in detuned loaded InGaAsP DBR lasers at 1.55 μm wavelength," *Electron. Lett.*, vol. 33, no. 6, pp. 488–489, 1997, doi: [10.1049/el:19970335](https://doi.org/10.1049/el:19970335).
- [25] Y. Mao et al., "Modulation bandwidth enhancement in distributed reflector laser based on identical active layer approach," *IEEE Photon. J.*, vol. 10, no. 3, Jun. 2018, Art. no. 1502308, doi: [10.1109/JPHOT.2018.2823739](https://doi.org/10.1109/JPHOT.2018.2823739).
- [26] Y. Matsui, R. Schatz, D. Che, F. Khan, M. Kwakernaak, and T. Sudo, "Low-chirp isolator-free 65-GHz-bandwidth directly modulated lasers," *Nature Photon.*, vol. 15, no. 1, pp. 59–63, 2021, doi: [10.1038/s41566-020-00742-2](https://doi.org/10.1038/s41566-020-00742-2).
- [27] H. N. Klein, H. Chen, D. Hoffmann, S. Staroske, A. G. Steffan, and K. O. Velthaus, "1.55 μm mach-Zehnder modulators on InP for optical 40/80 gbit/s transmission networks," in *Proc. IEEE Int. Conf. Indium Phosphide Related Mater. Conf.*, 2006, pp. 171–173.
- [28] O. Ozolins et al., "100 GHz EML for high speed optical interconnect applications," in *Proc. IEEE 42nd Eur. Conf. Opt. Commun.*, 2016, pp. 1–3.
- [29] S. Kanazawa et al., "Transmission of 214-gbit/s 4-PAM signal using an ultra-broadband lumped-electrode EADFB laser module," in *Proc. IEEE Opt. Fiber Commun. Conf. Exhib.*, 2016, pp. 1–3.
- [30] H. Mardoyan et al., "204-GBaud on-off keying transmitter for inter-data center communications," in *Proc. IEEE Opt. Fiber Commun. Conf. Expo.*, 2018, pp. 1–3.
- [31] J. Verbist et al., "First real-time 100-gb/s NRZ-OOK transmission over 2 km with a silicon photonic electro-absorption modulator," in *Proc. IEEE Opt. Fiber Commun. Conf. Exhib.*, 2017, pp. 1–3.
- [32] U. Troppenz et al., "40 Gbit/s directly modulated lasers: Physics and application," *Proc. SPIE*, vol. 7953, pp. 98–107, 2011.
- [33] D. Che et al., "Direct modulation of a 54-GHz distributed Bragg reflector laser with 100-GBaud PAM-4 and 80-GBaud PAM-8," in *Proc. IEEE Opt. Fiber Commun. Conf. Exhib.*, 2020, pp. 1–3.
- [34] M. Radziunas et al., "Improving the modulation bandwidth in semiconductor lasers by passive feedback," *IEEE J. Sel. Topics Quantum Electron.*, vol. 13, no. 1, pp. 136–142, Jan./Feb. 2007, doi: [10.1109/JSTQE.2006.885332](https://doi.org/10.1109/JSTQE.2006.885332).
- [35] J. Qi, Y. Xi, and X. Li, "Enhanced modulation bandwidth by exploiting photon resonance in push-pull modulated DFB lasers," in *Proc. IEEE Int. Conf. Numer. Simul. Optoelectron. Devices*, 2015, pp. 127–128.
- [36] J. Chen, R. Maciejko, and T. Makino, "Dynamic properties of push-pull DFB semiconductor lasers," *IEEE J. Quantum Electron.*, vol. 32, no. 12, pp. 2156–2165, Dec. 1996, doi: [10.1109/3.544763](https://doi.org/10.1109/3.544763).
- [37] M. C. Nowell and J. E. Carroll, "Push-pull modulated DFB lasers with low chirp and enhanced cut-off frequency for high speed systems," in *Proc. IEEE Colloq. High Capacity Opt. Commun.*, 1994, pp. 5/1–5/6.
- [38] D. D. Marcenac, M. C. Nowell, and J. E. Carroll, "Theory of enhanced amplitude modulation bandwidth in push-pull modulated DFB lasers," *IEEE Photon. Technol. Lett.*, vol. 6, no. 11, pp. 1309–1311, Nov. 1994, doi: [10.1109/68.334822](https://doi.org/10.1109/68.334822).
- [39] M. C. Nowell et al., "Low-chirp and enhanced-resonant frequency by direct push-pull modulation of DFB lasers," *IEEE J. Sel. Topics Quantum Electron.*, vol. 1, no. 2, pp. 433–441, Jun. 1995, doi: [10.1109/2944.401226](https://doi.org/10.1109/2944.401226).
- [40] B. J. Fianigan, J. E. Carroll, M. C. Nowell, and R. G. S. Plumb, "Improved resonance and chirp mechanisms for multigigabit/s push-pull modulated DFB lasers," *Proc. Inst. Elect. Eng.*, vol. 143, no. 1, pp. 49–56, 1996, doi: [10.1049/ip-opt:19960137](https://doi.org/10.1049/ip-opt:19960137).
- [41] J. Chi, X. Li, C. Niu, and J. Zhao, "Enhanced modulation bandwidth by delayed push-pull modulated DFB lasers," *Micromachines*, vol. 14, no. 3, 2023, Art. no. 633, doi: [10.3390/mi14030633](https://doi.org/10.3390/mi14030633).
- [42] R. Kazarinov and C. Henry, "Second-order distributed feedback lasers with mode selection provided by first-order radiation losses," *IEEE J. Quantum Electron.*, vol. 21, no. 2, pp. 144–150, Feb. 1985, doi: [10.1109/JQE.1985.1072627](https://doi.org/10.1109/JQE.1985.1072627).
- [43] J. Park, X. Li, and W.-P. Huang, "Gain clamping in semiconductor optical amplifiers with second-order index-coupled DFB grating," *IEEE J. Quantum Electron.*, vol. 41, no. 3, pp. 366–375, Mar. 2005, doi: [10.1109/JQE.2004.841495](https://doi.org/10.1109/JQE.2004.841495).
- [44] L. M. Zhang, S. F. Yu, M. C. Nowell, D. D. Marcenac, J. E. Carroll, and R. G. S. Plumb, "Dynamic analysis of radiation and side-mode suppression in a second-order DFB laser using time-domain large-signal traveling wave model," *IEEE J. Quantum Electron.*, vol. 30, no. 6, pp. 1389–1395, Jun. 1994, doi: [10.1109/3.299461](https://doi.org/10.1109/3.299461).
- [45] Y. Xi, X. Li, and W.-P. Huang, "Time-domain standing-wave approach based on cold cavity modes for simulation of DFB lasers," *IEEE J. Quantum Electron.*, vol. 44, no. 10, pp. 931–937, Oct. 2008, doi: [10.1109/JQE.2008.2000922](https://doi.org/10.1109/JQE.2008.2000922).
- [46] J. Chi, C. Niu, and J. Zhao, "Parameter extraction for quantum well DFB lasers based on 1D traveling wave model," *IEEE Photon. J.*, vol. 14, no. 5, Oct. 2022, Art. no. 1548508, doi: [10.1109/JPHOT.2022.3201578](https://doi.org/10.1109/JPHOT.2022.3201578).
- [47] S. Mieda, N. Yokota, R. Isshiki, W. Kobayashi, and H. Yasaka, "Frequency response control of semiconductor laser by using hybrid modulation scheme," *Opt. Exp.*, vol. 24, no. 22, pp. 25824–25831, 2016, doi: [10.1364/OE.24.025824](https://doi.org/10.1364/OE.24.025824).